Supplementary Information

Photochemical Processing of Dissolved Organic Matter in Fog Water: Oxidation and Functionalization Pathways Driving Organic Aerosol Evolution

Wenqing Jiang[1,2], Lijuan Li[1,3], Lu Yu[1,2], Hwajin Kim[1,4], Yele Sun[1,5], Qi Zhang[1,2]*

[1]Department of Environmental Toxicology, University of California, 1 Shields Ave., Davis, CA 95616, USA

[2]Agricultural and Environmental Chemistry Graduate Group, University of California, 1 Shields Ave., Davis, CA 95616, USA

[3] Research Center for Atmospheric Environment, Chongqing Institute of Green and Intelligent Technology, Chinese Academy of Sciences, Chongqing 400714, China

[4] Department of Environmental Health Sciences, Seoul National University, Seoul 08826, South Korea

[5] State Key Laboratory of Atmospheric Environment and Extreme Meteorology, Institute of Atmospheric Physics, Chinese Academy of Sciences, Beijing 100029, China

*Corresponding Author: Qi Zhang, Department of Environmental Toxicology, University of California, 1 Shields Ave., Davis, CA 95616, USA. Tel.: 530-752-5779; fax: 530-752-3394; e-mail: dkwzhang@ucdavis.edu

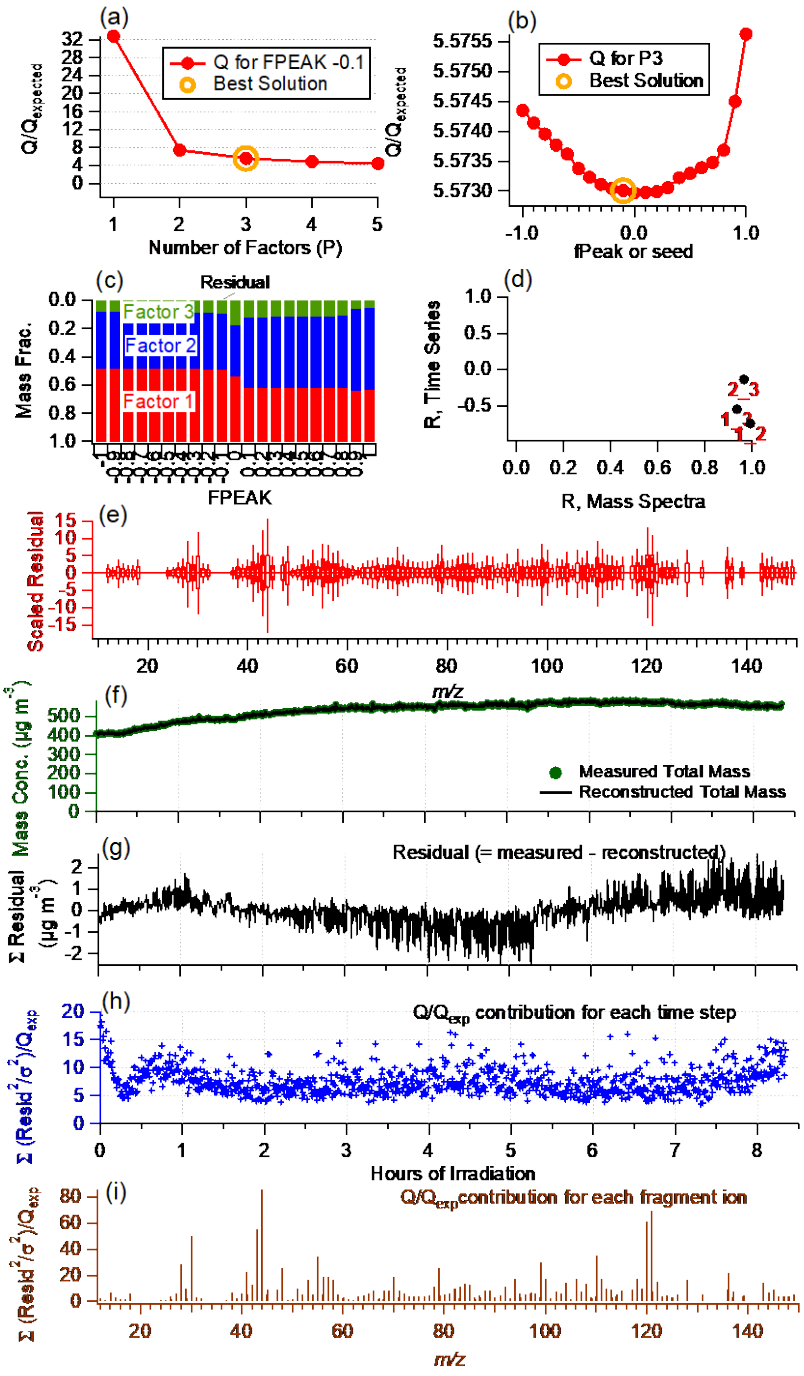

Figure S1. Summary of key diagnostic plots of the PMF results: **(a)** Q/Q_{exp} as a function of number of factors (p) selected for PMF analysis. For the best solution (3-factor solution) **(b)** Q/Q_{exp} as a function of *fPeak*, **(c)** fractions of PMF factors *vs*. *fPeak*, **(d)** correlations among PMF factors, **(e)** the box and whiskers plot showing the distributions of scaled residuals for each *m/z*, **(f)** time series of the measured organic mass and the reconstructed organic mass, **(g)** variations of the residual (= measured - reconstructed) of the fit, **(h)** the Q/Q_{exp} for each point in time, and **(i)** the Q/Q_{exp} values for each ion.

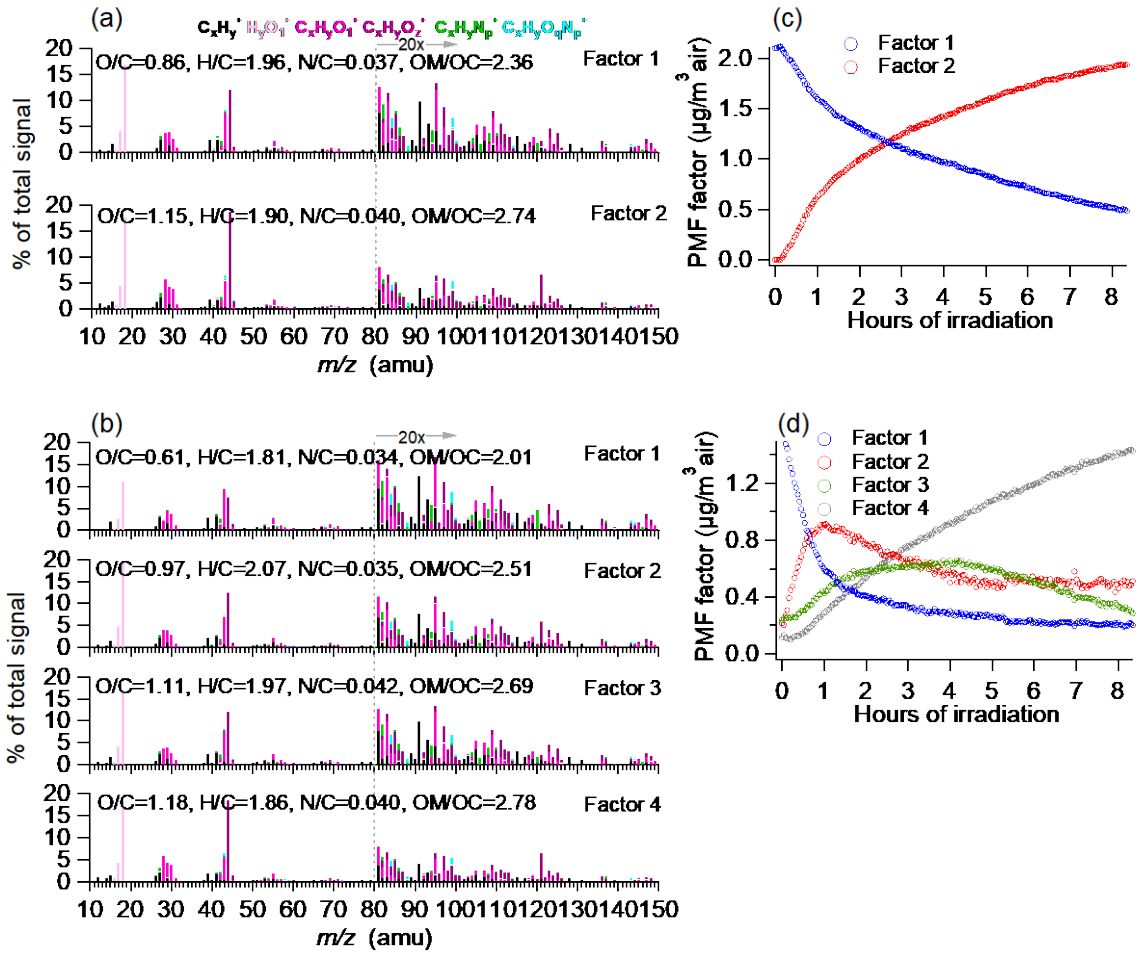

Figure S2. HR-AMS spectra for **(a)** two-factor PMF solutions and **(b)** four-factor PMF solutions. Peaks are colored by the six ion categories: $C_xH_y^+$, $H_yO_1^+$, $C_xH_yO_1^+$, $C_xH_yO_z^+$, $C_xH_yN_p^+$, and $C_xH_yO_qN_p^+$. The ion signals at $m/z_{\geq 80}$ are enhanced by a factor of 20 for clarity. The calculated atomic ratios are shown in the legends. Time series of **(c)** two-factor PMF solutions and **(d)** four-factor PMF solutions.

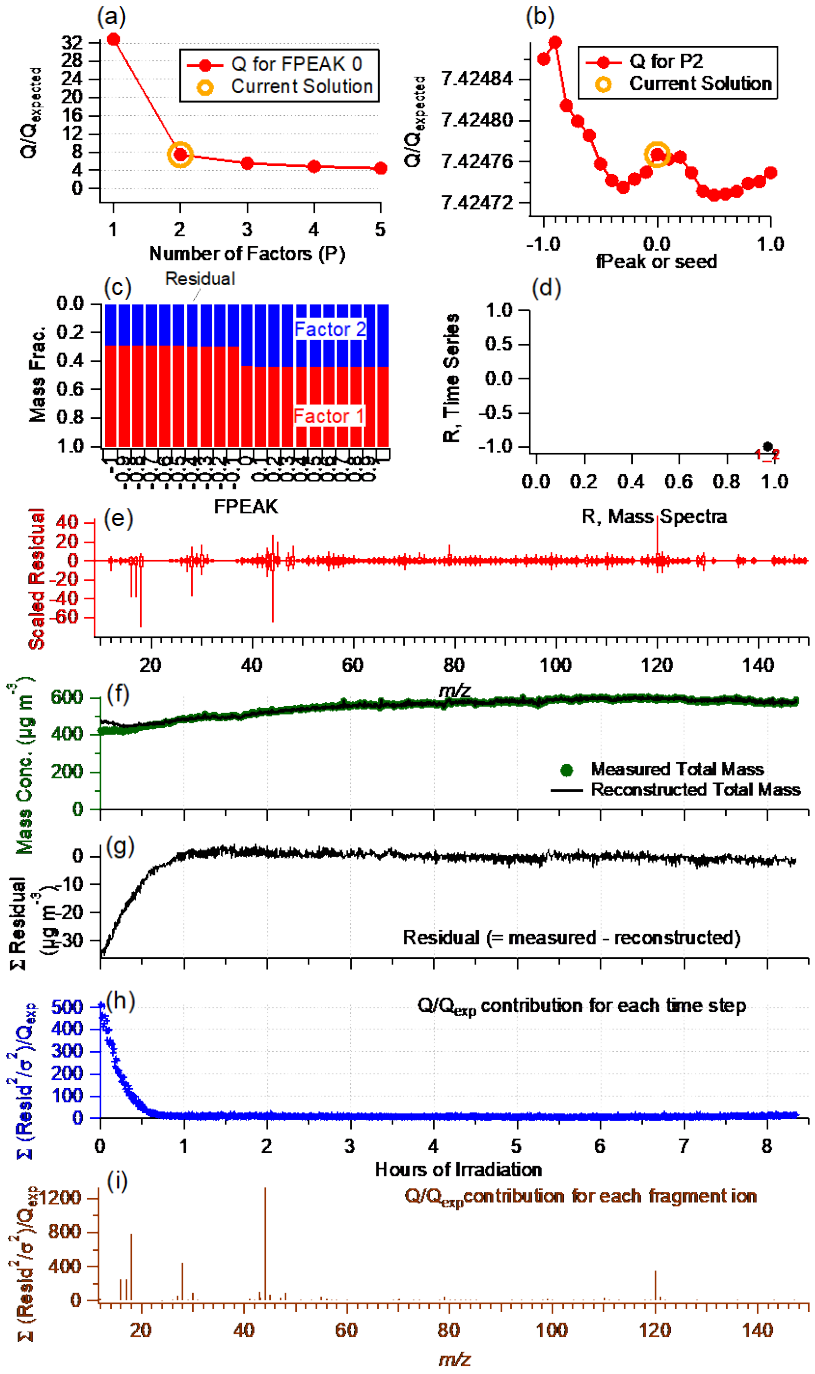

Figure S3. Summary of key diagnostic plots of the PMF results: **(a)** Q/Q_{exp} as a function of number of factors (p) selected for PMF analysis. For the 2-factor solution **(b)** Q/Q_{exp} as a function of *fPeak*, **(c)** fractions of PMF factors *vs*. *fPeak*, **(d)** correlations among PMF factors, **(e)** the box and whiskers plot showing the distributions of scaled residuals for each *m/z*, **(f)** time series of the measured organic mass and the reconstructed organic mass, **(g)** variations of the residual (= measured - reconstructed) of the fit, **(h)** the Q/Q_{exp} for each point in time, and **(i)** the Q/Q_{exp} values for each ion.

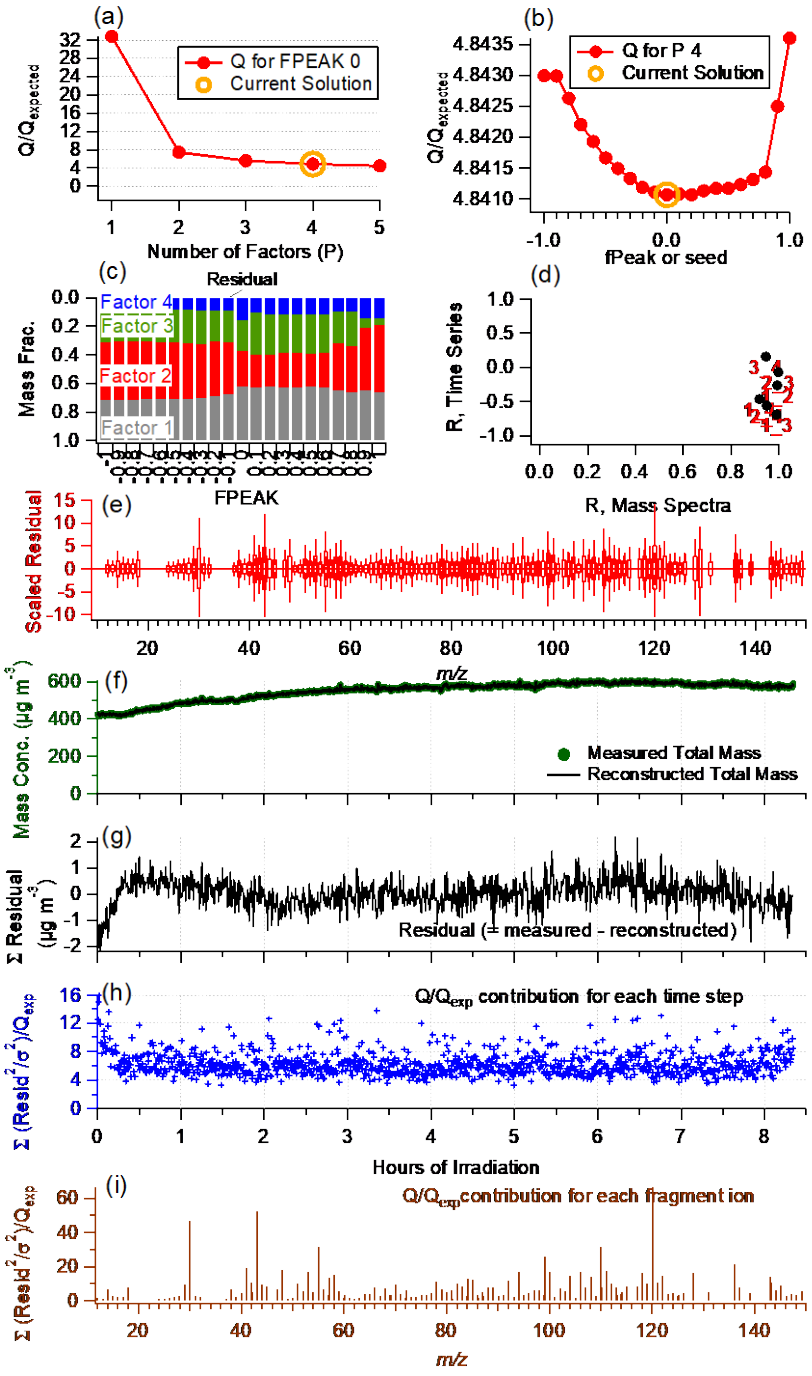

Figure S4. Summary of key diagnostic plots of the PMF results: **(a)** Q/Q_{exp} as a function of number of factors (p) selected for PMF analysis. For the 4-factor solution **(b)** Q/Q_{exp} as a function of *fPeak*, **(c)** fractions of PMF factors *vs*. *fPeak*, **(d)** correlations among PMF factors, **(e)** the box and whiskers plot showing the distributions of scaled residuals for each *m/z*, **(f)** time series of the measured organic mass and the reconstructed organic mass, **(g)** variations of the residual (= measured - reconstructed) of the fit, **(h)** the Q/Q_{exp} for each point in time, and **(i)** the Q/Q_{exp} values for each ion.

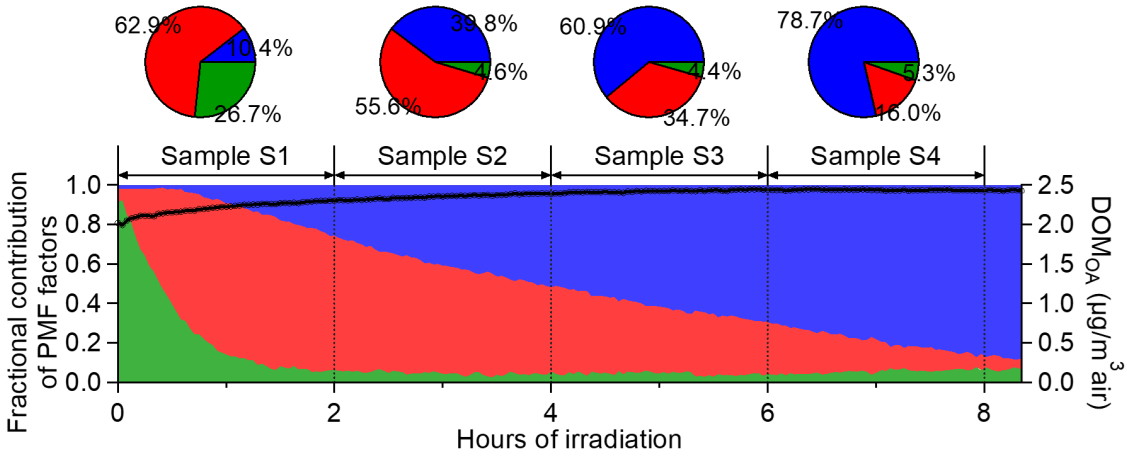

Figure S5. Fractional contributions of different PMF factors (from the 3-factor PMF solution) to DOM_{OA} in fog water samples collected at four irradiation intervals: S1 (0 – 2h), S2 (2-4 h), S3 (4-6 h) and S4 (6-8 h).

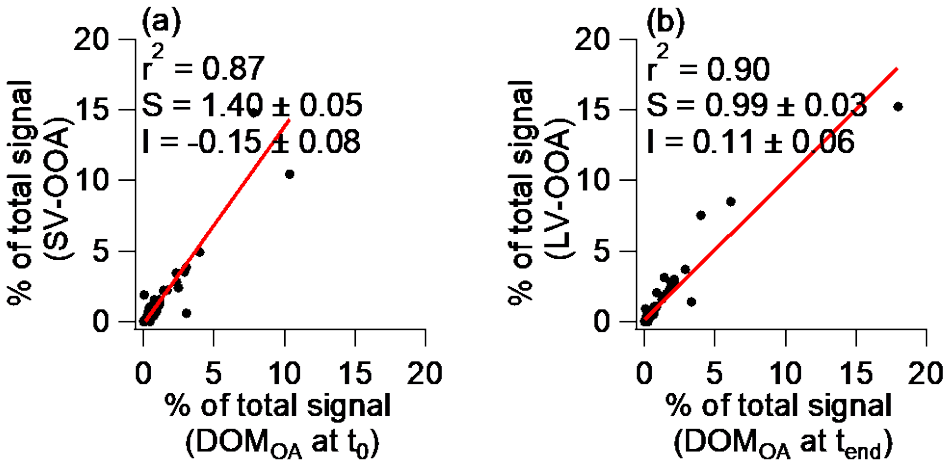

Figure S6. Scatter plots that compare the mass spectrum of SV-OOA and LV-OOA observed in ambient aerosols in Fresno in 2013 with the mass spectra of DOM_{OA} at t_0 and t_{end}, respectively. All linear regressions were performed using orthogonal distance regression (ODR) and the slopes (S), intercepts (I), and correlation coefficients (r^2) are shown in the legends.

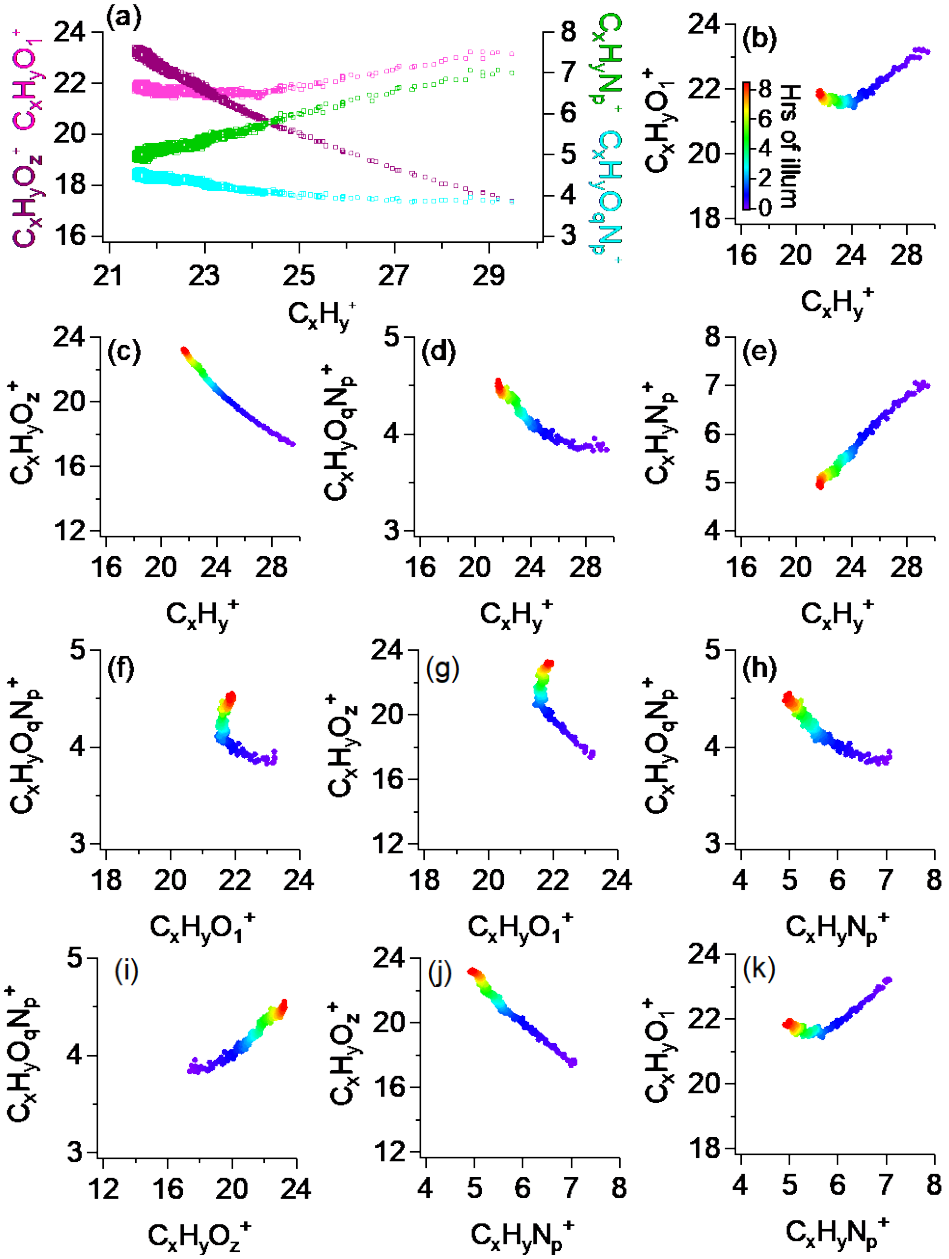

Figure S7. Correlations among signal contributions of major ion categories to DOM_{OA} spectra during simulated sunlight illumination. **(a)** Signal contributions (%) of $C_xH_yO_1^+$, $C_xH_yO_z^+$, $C_xH_yN_p^+$, and $C_xH_yO_qN_p^+$ plotted against $C_xH_y^+$ ($x \geq 1$; $y \geq 1$; $z > 1$; $p \geq 1$; $q \geq 1$). Each ion category is shown in a different color and symbol size scaled to irradiation time. **(b-k)** Pairwise correlations between the signal contributions (%) of $C_xH_yO_1^+$, $C_xH_yO_z^+$, $C_xH_yN_p^+$, $C_xH_yO_qN_p^+$, and $C_xH_y^+$. Data points are color-coded by hours of illumination (see color bar in b).

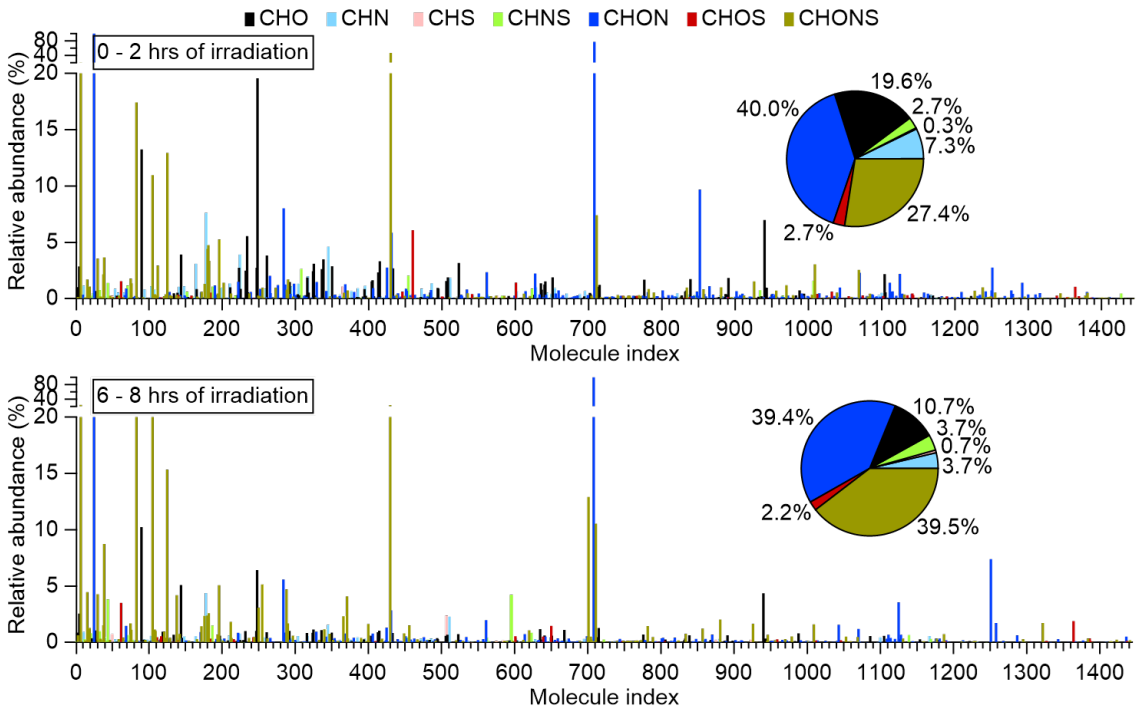

Figure S8. Molecular formulas detected by positive-mode ESI-MS in fog water samples collected during 0 – 2 hours (top) and 6 – 8 hours (bottom) of simulated sunlight irradiation. Bars display the relative signal intensities of individual molecular species, color-coded by elemental composition groups: CHO, CHN, CHS, CHNS, CHON, CHOS, CHONS. Accompanying pie charts summarize the fractional contributions of each group to the total signal.

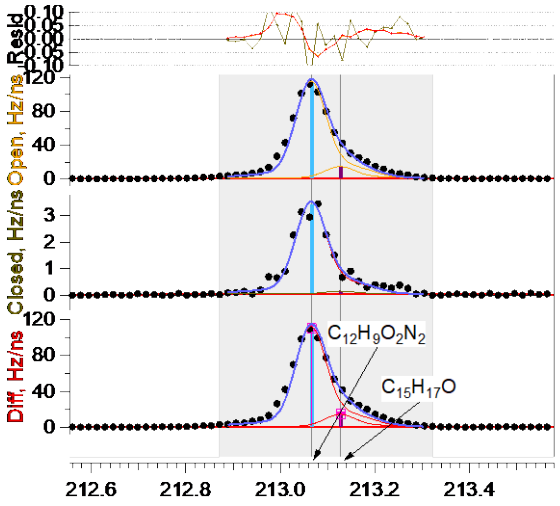
Resid
Open, Hz/ns
Closed, Hz/ns
Diff, Hz/ns
$C_{12}H_9O_2N_2$
$C_{15}H_{17}O$
212.6
212.8
213.0
213.2
213.4

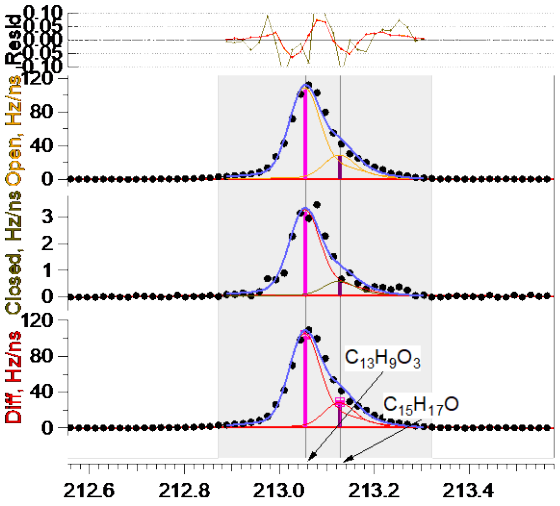
Resid
Open, Hz/ns
Closed, Hz/ns
Diff, Hz/ns
$C_{13}H_9O_3$
$C_{15}H_{17}O$
212.6
212.8
213.0
213.2
213.4

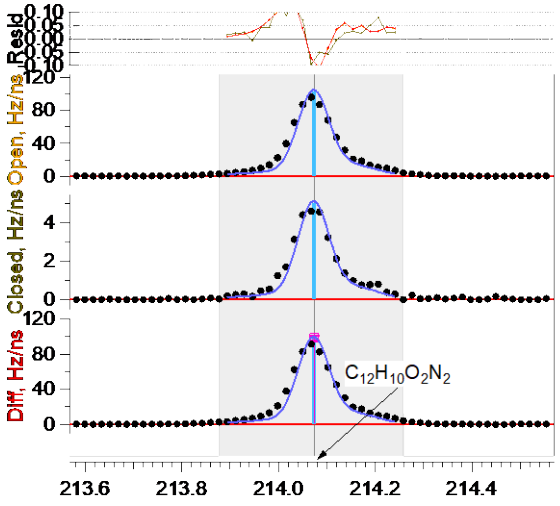
Resid
Open, Hz/ns
Closed, Hz/ns
Diff, Hz/ns
$C_{12}H_{10}O_2N_2$
213.6
213.8
214.0
214.2
214.4

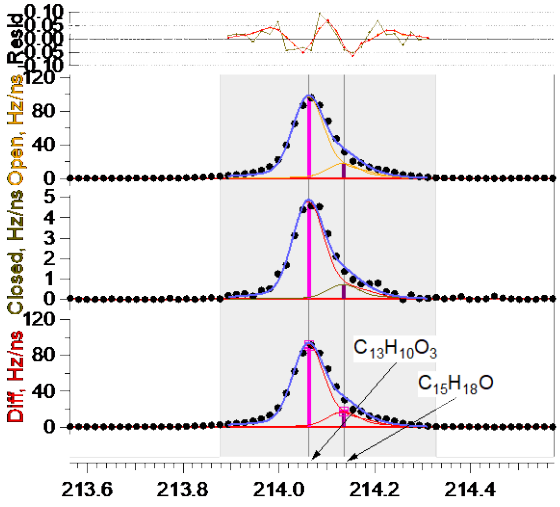
Resid
Open, Hz/ns
Closed, Hz/ns
Diff, Hz/ns
$C_{13}H_{10}O_3$
$C_{15}H_{18}O$
213.6
213.8
214.0
214.2
214.4

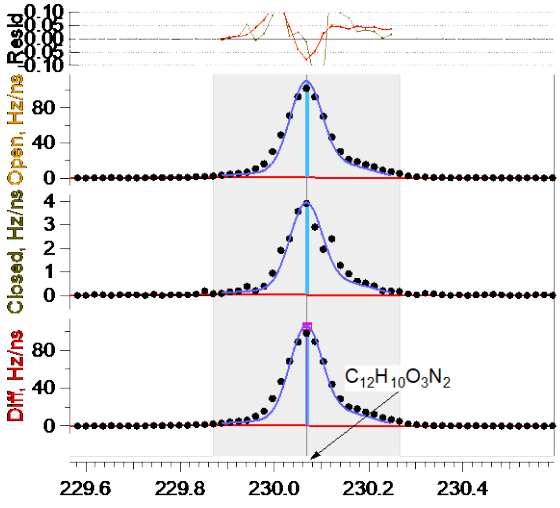
Resid
Open, Hz/ns
Closed, Hz/ns
Diff, Hz/ns
$C_{12}H_{10}O_3N_2$
229.6
229.8
230.0
230.2
230.4

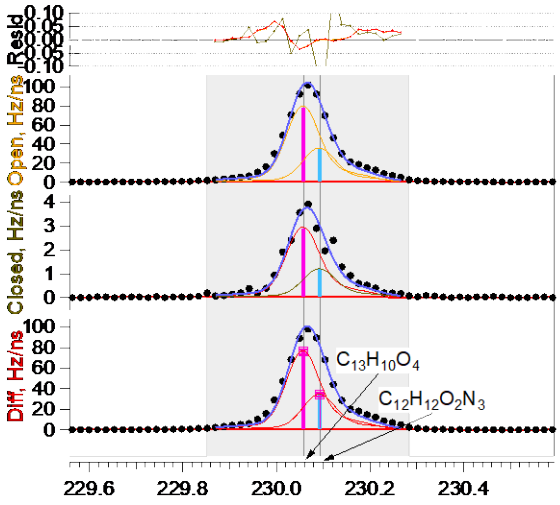
Resid
Open, Hz/ns
Closed, Hz/ns
Diff, Hz/ns
$C_{13}H_{10}O_4$
$C_{12}H_{12}O_2N_3$
229.6
229.8
230.0
230.2
230.4

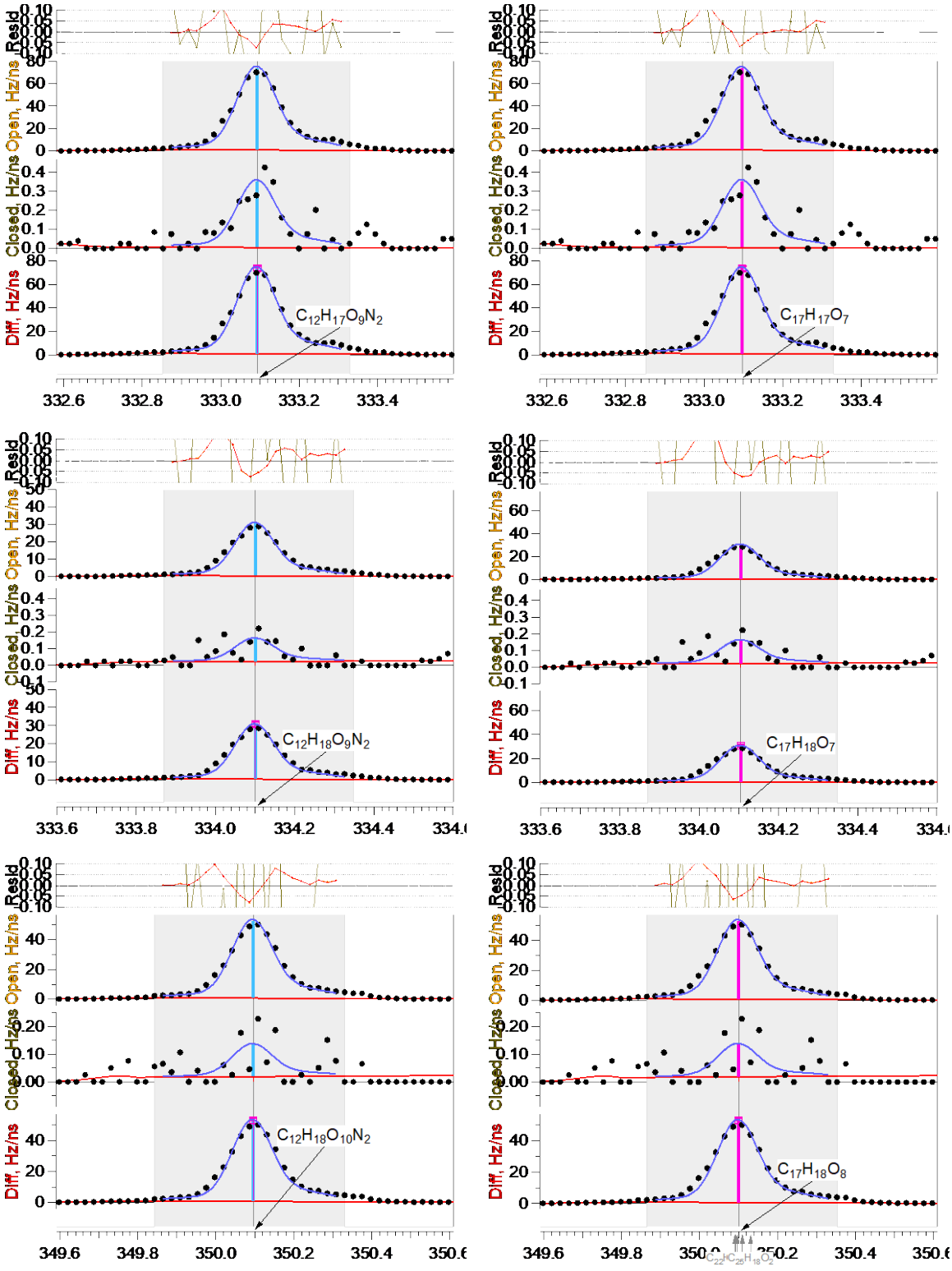

Figure S9. PIKA ion fitting of selected high *m/z* peaks in the HR-AMS spectra of DOM_{OA} at t_{end}. Panels display fitted ion signals at *m/z* 213, 214, 230, 333, 334, and 350. For each m/z, two fits are shown: the left panels assume elemental compositions containing C, H, O and N; the right panels assume compositions with only C, H, and O.

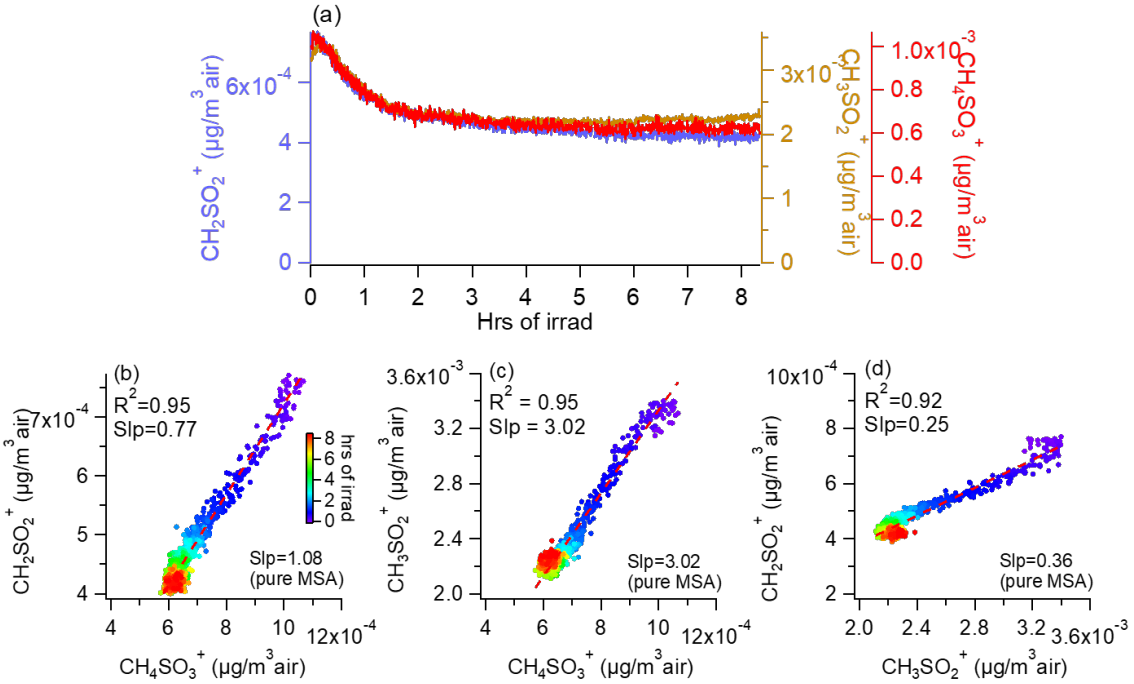

Figure S10. (a) Time trends of HR-AMS tracer ions for MSA (Ge et al. 2012), $CH_2SO_2^+$, $CH_3SO_2^+$, and $CH_4SO_3^+$, during simulated sunlight illumination. **(b -d)** Pairwise correlations among the three ions, with orthogonal distance regression (ODR) slopes (S), intercepts (I), and correlation coefficients (r^2) shown in each panel. Data points are color-coded by hours of illumination (see color bar in b).

References

Ge, Xinlei, Qi Zhang, Yele Sun, Christopher R. Ruehl, and Ari Setyan. 2012. “Effect of Aqueous-Phase Processing on Aerosol Chemistry and Size Distributions in Fresno, California, during Wintertime.” *Environmental Chemistry* 9(3):221–35.